Kufa Journal of Engineering
Vol. 11, No. 2, April 2020, P.P. 68-84
Received 5 October 2019, accepted 15 February 2020

STRUCTURAL, MECHANICAL AND THERMAL PROPERTIES OF LOW DENSITY POLYETHYLINE/BIOMASS COMPOSITE: EFFECTS OF PARTICLE SIZE

Oluwashina Gbenebor[1], Festus Osabumwenre[2] and Samson Adeosun[3]

[1] Department of Metallurgical and Materials Engineering, University of Lagos, Nigeria.

E-Mail: ogbenebor@unilag.edu.ng

[2] Department of Metallurgical and Materials Engineering, University of Lagos, Nigeria.
E-Mail: festusosabumwenre@yahoo.com

[3] Department of Metallurgical and Materials Engineering, University of Lagos, Nigeria.
E-Mail: sadeosun@unilag.edu.ng

http://dx.doi.org/10.30572/2018/KJE/110205

ABSTRACT

This study focuses on the use of Alibizia Lebbeck Benth pod particles (ALBp) as reinforcement on low density polyethylene (LDPE). Composites were processed via casting where 408 and150 µm ALBp where used in reinforcing LDPE. Samples were subjected to Fourier Transform Infrared Spectroscopy (FTIR), Scanning Electron Microscopy (SEM), X-Ray Diffraction (XRD), Differential Scanning Calorimetry (DSC). Thermogravimetry Analysis (TGA) impact strength and tensile characterizations. Composites showed improved thermal stability and crystallinity compared to unreinforced LDPE. Tensile strength (UTS) of composite increased by 331% as it improved from 0.36MPa for unreinforced LDPE to 1.55MPa using ALBp of 150µm. Additional C=C and C-O-C groups observed on the composite's spectrum could be responsible for the improvement in mechanical properties. Reinforcing LDPE with larger ALBp (408µm) culminated in the formation of gaps and voids in the composite.

KEYWORDS: Alibizia Lebbeck Benth; low density polyethylene; tensile strength; composite; crystallinity.

1. INTRODUCTION

Development necessitates the use of different kinds of materials in areas such as housing, clothing, transportation, medical, defence, food, etc. Success in materials development has recently propitiated the creation of advanced materials which includes polymer matrix composites (PMCs). Composites consist of more than one materials merged to create a lone piece with improved features compared to that of its individual components if used alone. Polymers are light in weight, adhere readily to other materials, flexible and easily processed to desired shapes due to their ease of flow at temperatures beyond its melting point (Sabu et al., 2012; Bilyeu et al., 2001). Often times, investigations affirm that mechanical properties of the matrix are being enhanced as a result of reinforcement inclusion which possesses better resistance to external loads (Adeosun et al., 2015). The reinforcement could either be fiber or particle. The particles could be spherical, platelets, or of any other regular or irregular geometry. Particle - reinforced composites are less expensive than fiber reinforced composites and in addition, they usually require less reinforcement (up to 40 to 50 wt. %) due to processing difficulties and ease of fracture (Uygunoglu et al., 2012). Particle – reinforced polymers have been found useful in manufacturing, electrical, commercial and aviation industries (Kim et al., 2004). Polymeric materials that have been used as matrix include synthetic polymers such as epoxy resins, polyethylene, polypropylene, unsaturated polyester 5 and biopolymers such as polylactide (Wan et al., 2004; Gupta et al., 2001; Shehu et al., 2014; Huang et al., 2013; Flandez et al., 2012; Adeosun et al., 2016). Fillers sourced from nature have been proven to yield nontoxic products and impart mechanical strength on plastics owing to their high stiffness (Ishidi, 2014) compared to the synthetic ones including carbon and glass fiber.

During the last few years, biomass from crops has been the main target in the search for new materials applicable in several industrial areas. These materials however, are ubiquitous and hence cheap to source, easily interact with matrix and offer good thermal properties (Raju et al., 2012). The filler used for this study is sourced from Albizzia lebbeck Benth (ALB). This tree is being regarded as “all purpose” tree and belongs to leguminosae family and widely distributed in Asia, South Africa, Australia and West Africa (Nazneen et al., 2012). The plant is often used in medicine because it possesses antimicrobial and antioxidant features (Shahid and Firdou, 2012). The use of this plant as a reinforcement in polymer has not been explored. Pods of ALB often litter the environment when detached from the stalk (result of ripening) and are mostly being discarded. This study examines the potential of converting these perceived

wastes to useful materials for engineering applications by investigating the influence of ALB pods particles on the mechanical properties of LDPE.

2. MATERIALS AND METHOD

2.1. Materials

TASNEE LD 1925AS pellets with melt flow rate 1.9g/min and density of 0.925g/cm^3 was used for this experiment.

2.2. Preparation method

Dry pods of ALB were gathered and milled to particle sizes of 408 and150μm. Particle of 30 wt. % was measured as reinforcement contents introduced to the LDPE matrix. Materials were charged into the heating chamber of a compounding machine designed for this work. Thorough ALBp distribution in molten LDPE was achieved via stirring powered by electric motor. The mixture was poured into moulds after LDPE had reached its molten state.

2.3. Characterizations

2.3.1. Fourier Transform Infrared spectroscopy (FTIR)

Functional groups in matrix, reinforcement and composite were detected with the use of Nicolet 6700M spectrometer. Each sample of 10mg was compressed to pellets after being dispersed in KBr Spectra measurement in absorbance mode were processed at a resolution of 4 cm^{-1} between 500–4000 cm^{-1}.

2.3.2. Water absorption

Dry samples were initially weighed and immersed in distilled water at 32˚C for 8 weeks. At the end of each week, soaked samples were separated from the medium, cleaned to remove surface moisture and weighed. The quantity (%) of the water absorbed by LDPE and composites in terms of weights measured were calculated using Equation 1.

$$\text{ABS}(\%) = \frac{\text{Ww}-\text{Wd}}{\text{Wd}} \text{ x } 100 \qquad 1$$

Quantity of water absorbed, weights before and after immersion are represented by *Abs*, *Wd* and *Ww* respectively.

2.3.3. Thermal test

Differential Scanning Calorimetry (DSC) and Thermogravimetric Analysis (TGA) were used in determining thermal characteristics of samples. With the use of a Mettler Toledo DSC

equipment, samples were appropriately weighed and heated from 0 to 150 ºC at the rate of 10 ºC/min where flow of heat was plotted against temperature. Crystallinity (X_c) was calculated using Equation 2 (Chun et al., 2015):

$$X_c\,(\%) = \left(\frac{\Delta H_f}{\Delta H_f^o}\right) \times 100 \qquad 2$$

Samples' heat of fusion is given by H_f while that of fully crystalline LDPE (taken as 288 J /g) is represented by ΔH_f^o.

Samples assigned for TGA analysis were heated from 25ºC to 600ºC at a similar rate with that of DSC with the use of Shimadzu - DTG-60 equipment in a nitrogen atmosphere purged at 50 ml/min. Thermogravimetric curves were plotted from the results.

2.3.4. X-Ray Diffraction (XRD)

A PANanalytical Empyrean was used for this study and samples were exposed to a monochromatic Cu Kα radiation (k = 1.5406), operating at 40 kV and 40 mA. The X_c was calculated from the height ratio in the diffractogram having crystalline (*Ic*) and amorphous (*Iamr*) peak intensities relationship using Equation 3 (Abdul Rahman et al., 2017).

$$Xc\,(\%) = \left(\frac{Ic - Iamr}{Ic}\right) \times 100 \qquad 3$$

From the XRD result, relationship among the incident radiation wave length (, in angstrom), width of crystalline peak at half height (, in radians) and Bragg's angle (, in degree) was used in determining the D_{hkl} values of samples by employing Equation 4 (Wang et al., 2013).

$$Dhkl = k\lambda / \beta\cos\theta \qquad 4$$

Indication of crystallite perfection is denoted by *K*, usually taken to be 1 while possesses a default magnitude of 1.5406. The equation above calculates the crystallite sizes of samples.

2.3.5. Tensile test

Tensile specimens were prepared and tested in accordance with ASTM D412 with the use of an Instron Tensometer. Each sample was fixed and held firmly at both ends by the gauge and load was applied at 10 mm/min at room temperature until the sample finally failed. The tensile strength (UTS) and extent of deformation response were measured from the stress-strain results recorded.

2.3.6. Impact test

An impact testing equipment (Izod) was used in determining the shock absorbing strength of samples in conformity with ASTM D256.

2.3.7. Scanning Electron Microscopy (SEM)

Samples to be investigated for morphological studies were coated win Au to enhance proper electrical conductivity which were scanned using a Phenom Prox. 800-7334 model SEM.

3. RESULTS AND DISCUSSION

3.1. FTIR

The FTIR spectrum of ALBp in Fig. 1a shows a strong band at 3406 cm^{-1}, displaying free hydroxyl groups (OH) available in the biomass. Bands are observed at 2928 cm^{-1} for C–H stretching, 1754 cm^{-1} for C=O ester, 1643 cm^{-1} for C=C in alkenes, 1460 cm^{-1} for C–H bending, 1236 and 1056 cm^{-1} for C–O–C stretching of ester. The FTIR spectrum of unreinforced LDPE between 4000 and 500 cm^{-1} shown in Fig. 1b has the characteristic absorbance at 3439 cm^{-1} implying OH bending. Strong CH_2 and weak CH_3 symmetric stretching occurs at 2860 and 1377 cm^{-1} respectively while assymetric stretching and bending of CH_2 is absorbed at 2918 and 1464 cm^{-1} respectively. Twisting deformation of CH_3 is absorbed at 1301cm^{-1}. Comparing the spectrum of 70LDPE/30ALBp composite (Fig. 1b) with that of LDPE, the OH group occupies a wider region at 3422cm^{-1} which could be as a result of cellulose and hemicellulose present in ALBp. Additional peaks of 1644 (C=C) and 1057cm^{-1} (C-O-C) will impart improved mechanical strength on the composite.

3.2. Water absorption

Amount of water absorbed by all samples during 8 weeks of immersion illustrated in Fig. 2, increases until equilibrium conditions are reached. Unreinforced LDPE exhibits the least magnitude of water absorption while result shows that ALBp enhances significant water absorption in the composites during the immersion period. As evidenced in the FTIR spectrum of 70LDPE/30ALBp shown in Fig. 1b, the amount of free OH groups in ALBp has engendered water absorption of composites. These free OH groups form hydrogen bonding, when combined with water and thus culminate in weight gain of composites. In addition, reinforcing LDPE with a larger ALBp size of 408 µm as used in this study hastens degradation of 70LDPE/30ALBp as it produces a wider contact area for water molecules. Poor wettability promoted by these

large particles may have also encouraged penetration of water molecules through the composites' structures.

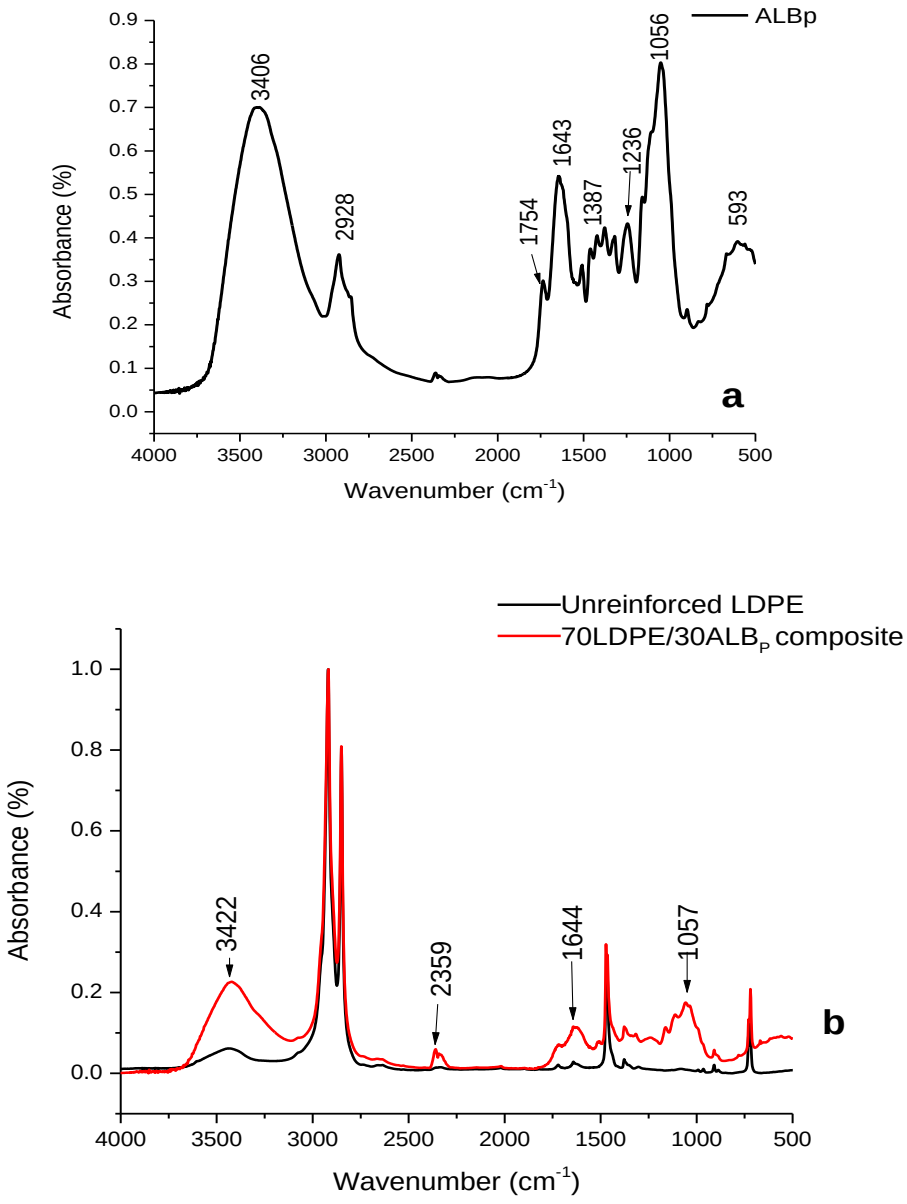

Fig. 1. FTIR spectra of (a) ALBp (b) unreinforced LDPE and 70LDPE/30ALBp composite.

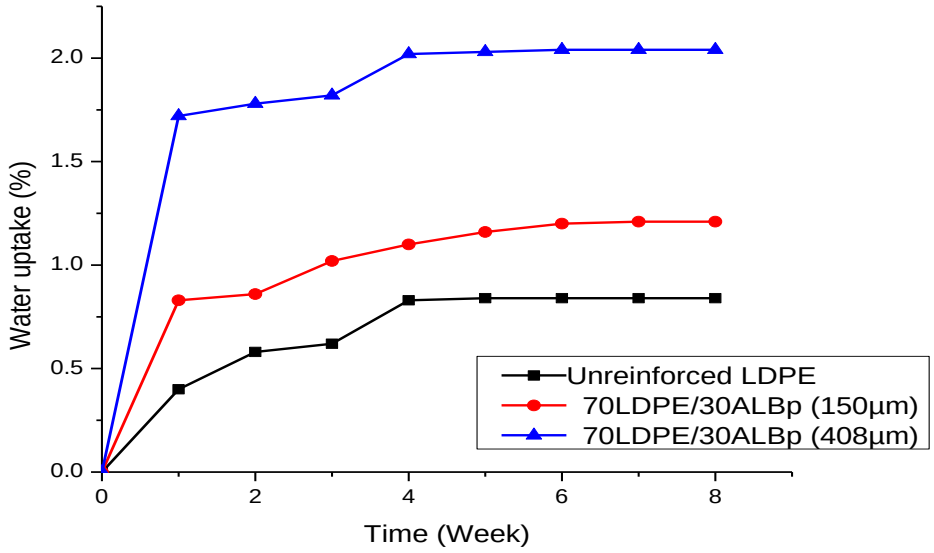

Fig. 2. Water absorption of unreinforced LDPE and 70LDPE/30ALBp composites at 150 and 408 µm particle sizes.

3.3. TGA

A single step decomposition of LDPE is observed within 453 – 477°C in the TGA and DTG curves shown in Fig. 3a and b. Comparing this with 70LDPE/30ALBp composites, the curves are characterized by two-step decomposition. This entails the decomposition of volatile compounds and hemicellulose in ALBp between 320 - 349°C (first step) and followed by decomposition of lignin and cellulose in 70LDPE/30ALBp (second step). The composites display a delayed thermal degradation as both 70LDPE/30ALBp at 150 and 408µm exhibit temperature at onset of degradation (T_{onset}) at 460°C compared to unreinforced LDPE whose T_{onset} is 453°C. The temperature at which the decomposition is maximum (T_{max}) are 458, 481 and 475°C for unreinforced LDPE, 70LDPE/30ALBp (150µm) and 70LDPE/30ALBp (408µm) composites respectively (Fig. 3b). This further justifies a slight improvement in the thermal stability of LDPE/ALBp composites which could be attributed to the residue formed during the heating process of ALBp which serves as barrier that prevents the thermal degradation of composites. Table 1 shows the Tonset, Tfinish Tmax and residue content obtained from the thermal investigation.

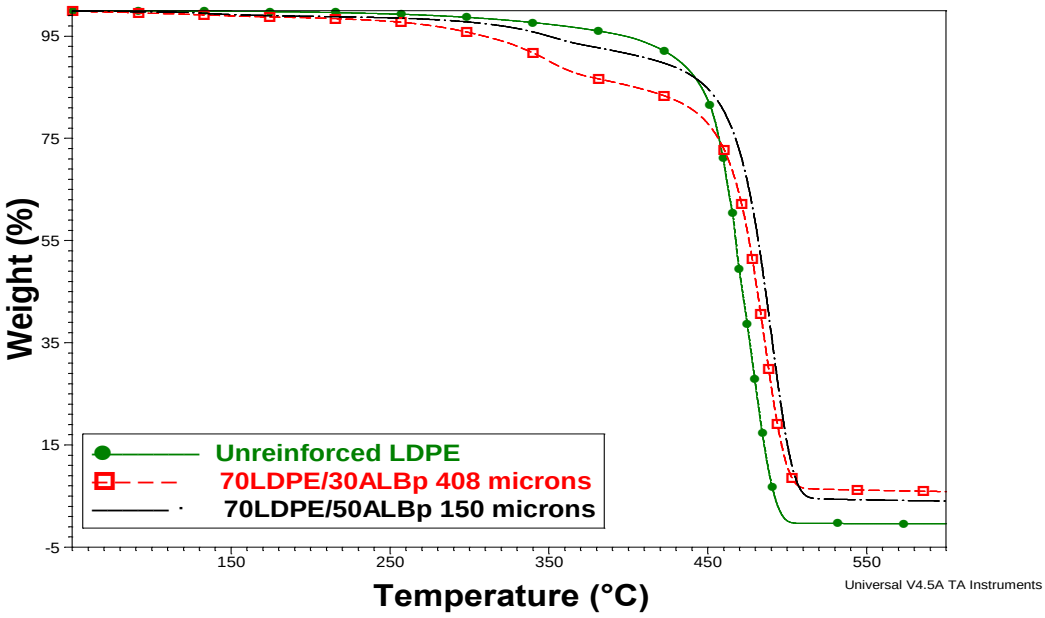

a

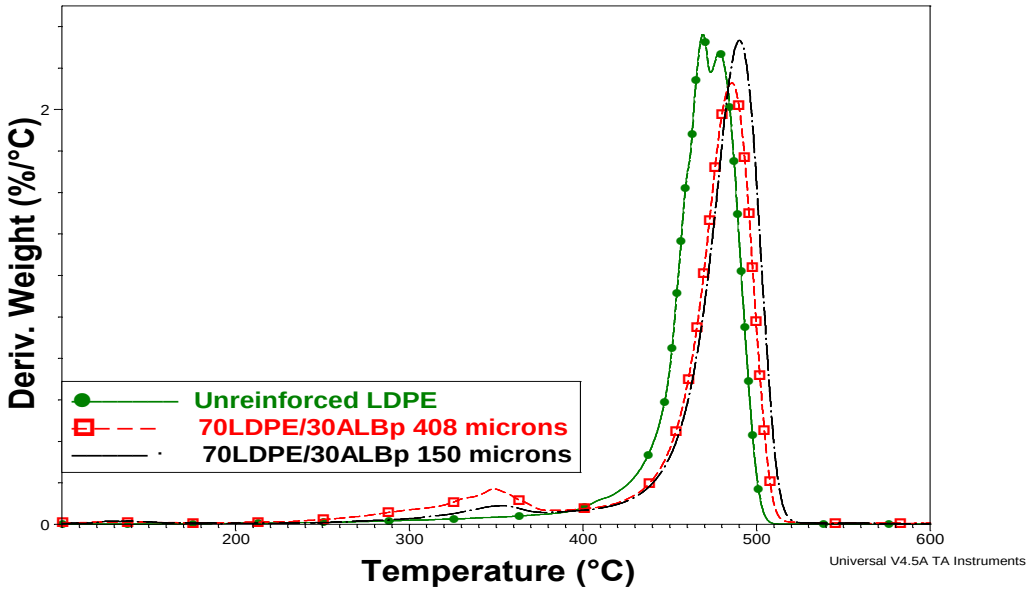

b

Fig. 3. (a) TG and (b) DTG of LDPE and 70LDPE/30ALBp composites at 150 and 408 µm particle sizes.

Table 1. TGA data summary of samples.

Samples	T_{onset} (°C)	T_{offset} (°C)	T_{max} (°C)	Residue (%)
Unreinforced LDPE	453	477	458	0
70LDPE/30ALBp (150 µm)	460	488	481	13.2
70LDPE/30ALBp (408 µm)	460	489	475	6.9

3.4. DSC

Fig. 4 shows the DSC of unreinforced LDPE and that reinforced with ALBp of 408 and 150µm sizes. The melting temperature (T_m) of samples is not significantly affected as there exists1-2°C increase from 111°C T_m recorded by unreinforced LDPE (see DSC data of samples summarized in Table 2). Both particles show significant effect on LDPE with increase in *Xc* as a result of interfacial bonding between matrix and reinforcement. However, 70LDPE/30ALBp (150µm) exhibits a higher X_C of the two composites .This heightens as a result of the presence of finer ALBp which has initiated proper wetting of matrix and reinforcement which entails diffusion of LDPE to ALBp surface. Thus, matrix/reinforcement interaction is more favourable in the finer particle (150µm) compared to a much coarse ALBp of 408µm.

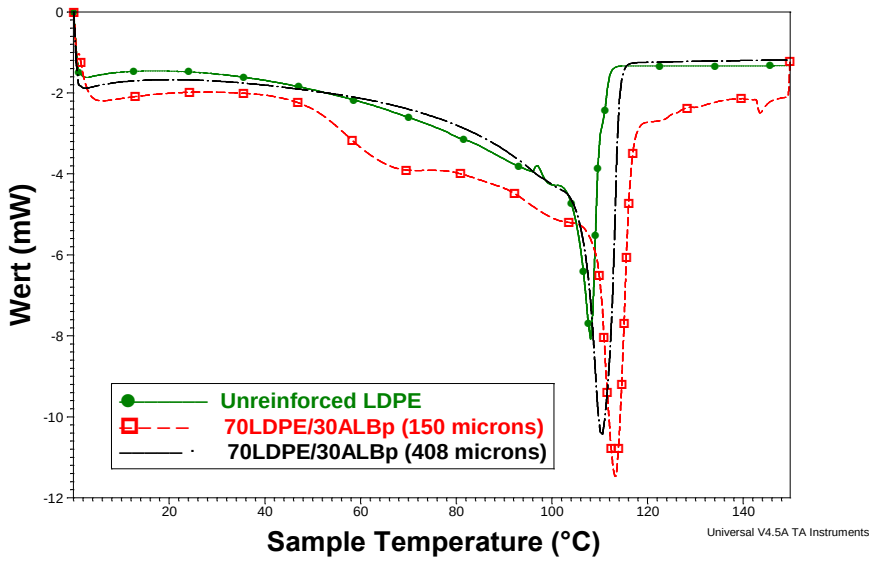

Fig. 4. DSC of unreinforced LDPE and 70LDPE/30ALBp composites at 150 and 408 µm particle sizes.

Table 2. DSC results of samples.

Samples	T_m (°C)	(J/g)	*Xc* (%)
Unreinforced LDPE	111	80	28
70LDPE/30ALBp (150 µm)	113	95	33
70LDPE/30ALBp (408 µm)	112	90	31

3.5. XRD

The diffractogram of ALBp exhibits a typical crystalline structure of native cellulose (Fig. 5a), where peak at 2θ = 22º corresponding to (002) crystallographic plane exists. In addition, there lies a broad band between 2 θ = 30º and 58º. Deconvolution of this broad band via Gaussian method (until maximum F number >10,000, which corresponds to a R^2 value of 0.99) reveals that two peaks are diffracted at 2 θ = 34.5º and 44.9º. The broader, (44.9º) which represents the amorphous peak is due to the presence of hemicellulose and lignin. The second crystalline peak at 2 θ = 34.5º in ALBp is represented by (040) crystallographic plane. The *X*c of cellulose that can be obtained in ALBp as calculated using Equation 2 is 46.9%. Comparing this with *X*c calculated using the area of deconvoluted peaks using Equation 5,

$$Xc = \frac{A002+A040}{A002+A040+Aamr} \times 100 \qquad 5$$

Where *A020*, *A040* and *Aamr* represent areas under the crystalline (for (002) and (040)) and amorphous peaks respectively. The *X*c is calculated to be 47.1% which is comparable to that obtained using the peak intensity method. This gives the amount of crystallinity of cellulose that can be obtained in ALB pods in an untreated state.

The XRD patterns of unreinforced LDPE and 70LDPE/30ALBp composites are shown in Fig. 5b with two distinct peaks. Each sample exhibits typical diffraction peak of LDPE where the stronger peak (representing (110) plane) exists at 2 θ = 21.6º, 20.6º and 21.4º for unreinforced LDPE and the polymer composite possessing 408 and 150µm particles respectively. The peak diffraction on (200) plane ranges between 22.9º – 23.8º for each sample. Reinforcing LDPE with ALBp engenders narrower peaks with greater intensity compared to unreinforced LDPE diffraction peaks. This is an indication of improved crystallinity which is calculated from DSC results in this study (see Fig. 4). Comparing the two composites, reinforcement with a finer ALBp of 150µm shows much narrow diffraction patterns than that reinforced with 408µm ALBp. It can thus be said that the presence of cellulose in ALB enhances the molecular chain arrangement of LDPE which is better improved with a finer one. The improved crystalline sizes (increase in magnitude) of 70LDPE/30ALBp composite compared to unreinforced LDPE suggests that *X*c of composites should be higher with 70LDPE/30 ALBp (150µm) possessing the highest of the three samples. This is illustrated in Table 3.

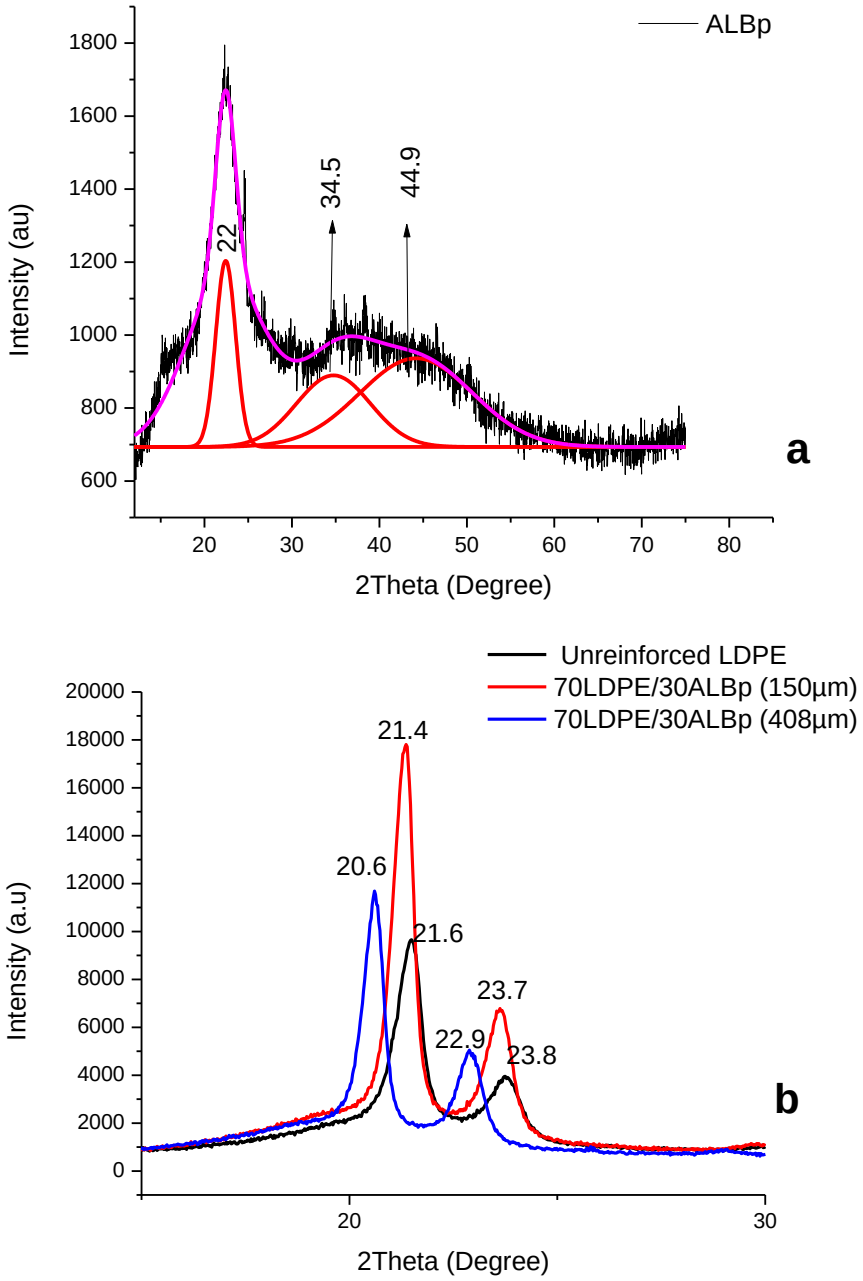

Fig. 5. XRD of (a) ALBp (b) 70LDPE/30ALBp composites at 150 and 408μm particle sizes.

Table 3. Crystalline size of samples.

Samples	D_{020} (nm)	D_{040} (nm)
Unreinforced LDPE	682	896.1
70LDPE/30ALBp (150 μm)	781	10.3
70LDPE/30ALBp (408 μm)	735	978.7

3.6. Tensile test

The experimental results in Fig. 6 reveal that the reinforcement used have significantly created strengthening effect on LDPE, which is responsible for the steady increase in UTS compared

to the unreinforced sample (100 wt. % LDPE). This property improves from an initial strength of 0.36MPa in unreinforced LDPE to 1.07 and 1.55MPa when reinforced with 408 and 150μm ALBp respectively. There is a sudden drop in stress of the two composites after UTS have been exceeded. The volume fraction of the reinforcement (which is less elastic than the matrix) used in this study has acted as a rigid constituent which obstructs the mobility of crazes. Gradual load increase is thus required during the deformation process until the maximum strength is reached. Beyond this point, there will be matrix/filler de-bonding caused by reduction in inter particle spacing which must have led to such drop. Effect of the ALBp on strain at break, whose percentage is a function of samples' ductility, is also illustrated in Fig 6. Ductility of 70LDPE/ 30ALBp composites is lower than unreinforced LDPE, measured to be 9.5%. Addition of particulates may have caused the matrix to lose its elastic properties. Incorporation of 30 wt. % of 150 and 408μm ALBp into LDPE matrix both reduce the elongation at break to 8.9%. It can be concluded that the reinforcement acts a rigid constituent which obstructs the mobility of craze during the deformation process. Ductility of LDPE is reduced to the same magnitude on addition of ALBp irrespective of the different particle sizes.

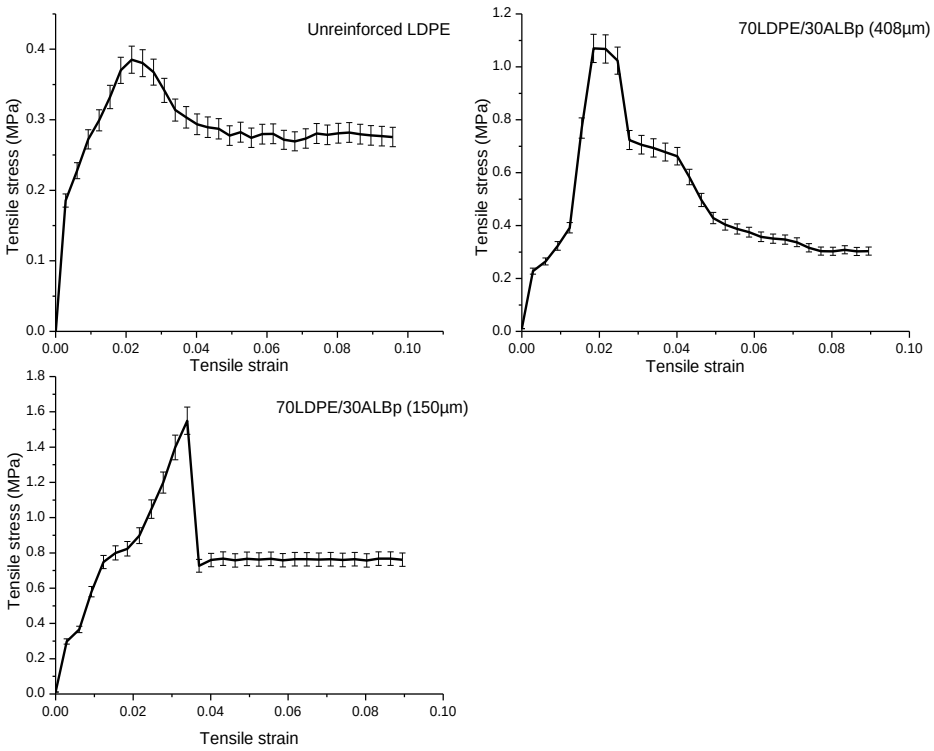

Fig. 6. Stress-strain graphs of LDPE and 70LDPE/ 30ALB$_p$ composites at 150 and 408 μm particle sizes.

3.7. Impact test

The energy absorbed on sudden load application on samples is shown in Fig. 7. Impact strength of LDPE is improved due to favourable interfacial bonding existing between the filler and the

matrix. This prevents the occurrence of micro-cracks from occurring at the point of impact. This figure shows that impact energy of sample is elevated from 19.5J in unreinforced LDPE to 20.8 and 22.0J in 70LDPE/30ALBp (408 µm) and 70LDPE/30ALBp (150 µm) composites respectively. This implies that the finer the ALBp the better they act as terminator of craze, which will contribute to the improvement of composites' impact strengths.

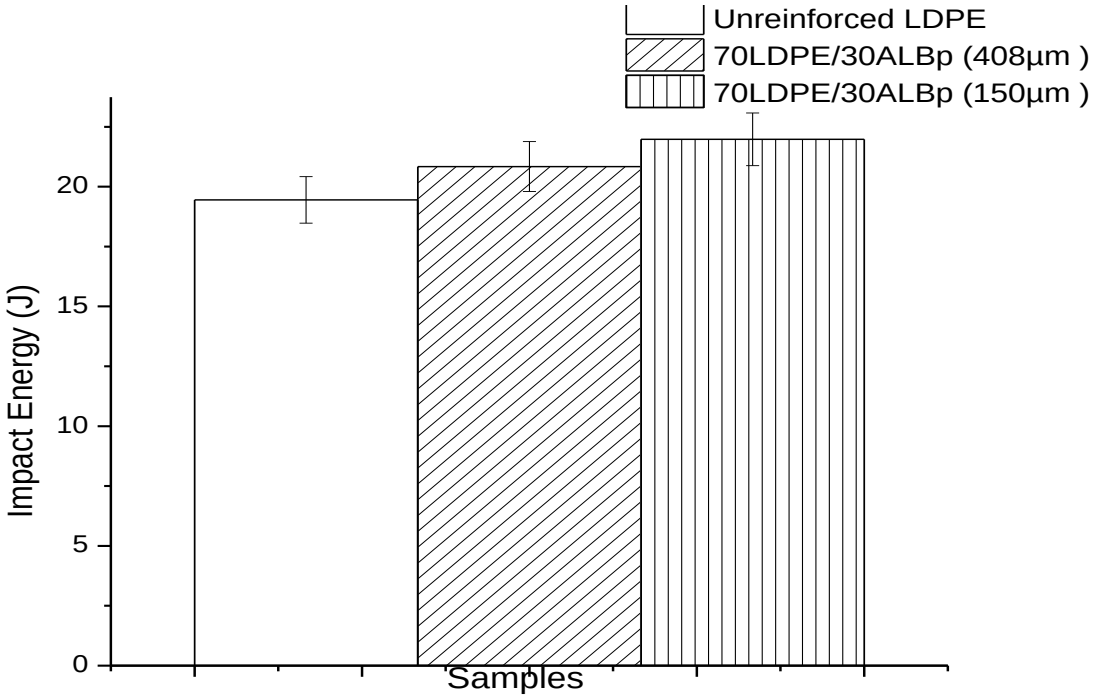

Fig. 7. Impact strengths of LDPE and 70LDPE/ 30ALB$_p$ composites at 150 and 408 µm particle sizes.

3.8. SEM

A defect free micrograph of 100 wt. % LDPE fractured surface is shown in Fig. 8a with low degree fibrils following a defined orientation. This could be an evidence of directional crystallization during curing. Addition of ALBp to LDPE increases degree of fibrils with definite geometry. Comparing micrograph of 100 wt. % LDPE to the fractured surface of 70LDPE/30 ALBp,(150µm) an improved reinforcing effect is observed as directional plate-like fibrils clamping over each other (in steps) is formed (Fig. 8b) with even distribution of reinforcement in its structure devoid of particles detachment. The good 70LDPE/30ALBp (150µm) interfacial bonding is accountable for its superlative UTS. Existence of gaps and cavities as a result of particle detachment after fracture is shown in Fig. 8c. This shows that interfacial adhesion between the LDPE and 408µm ALBp reinforcement is poor.

These defects are initiators of cracks in LDPE which have culminated in their lowest magnitudes of impact energies when compared to LDPE reinforced with 150µm ALBp. Fig. 9a, b and c shows the fractured morphologies of samples after the immersion period. Bump-

like feature of unreinforced LDPE (Fig. 9a) is an evidence of polymer swelling which is uniform throughout the sample. The swollen bumps are indication of distortion of polymer's molecular arrangement. Fibril steps in fractured surfaces of LDPE reinforced with 150µm ALBp in Fig. 8b gradually wears off while there is further surface roughening characterized by expansion of voids in 70LDPE/ 30ALBp (408 µm) sample as shown in Fig. 9c; these are indications of matrix/filler de-bonding.

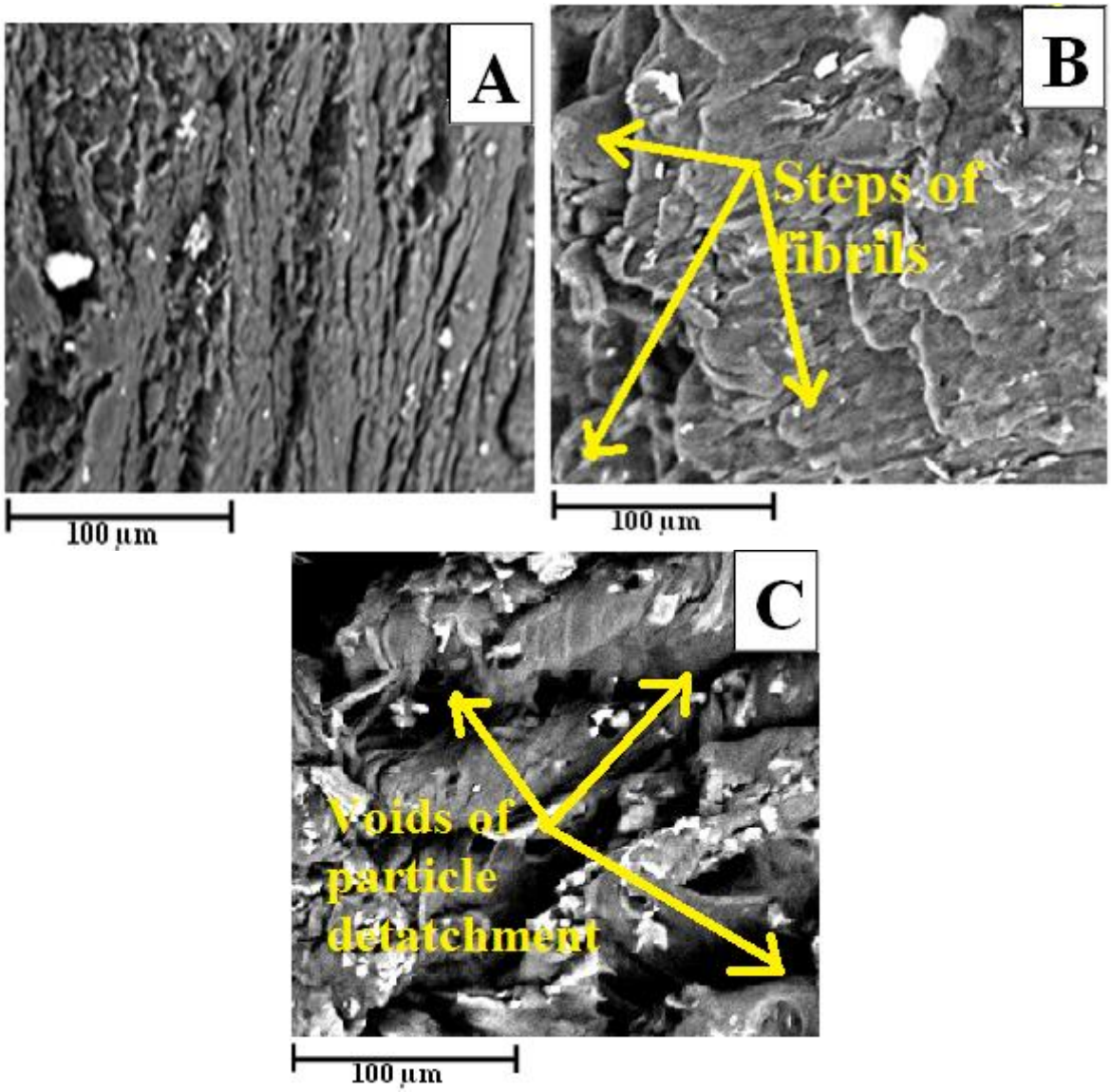

Fig. 8. Fractured tensile test SEM images of (a) unreinforced LDPE (b) 70LDPE/30ALB$_p$ (150µm) (c) 70 LDPE/30 ALBp (408 µm) before immersion in water.

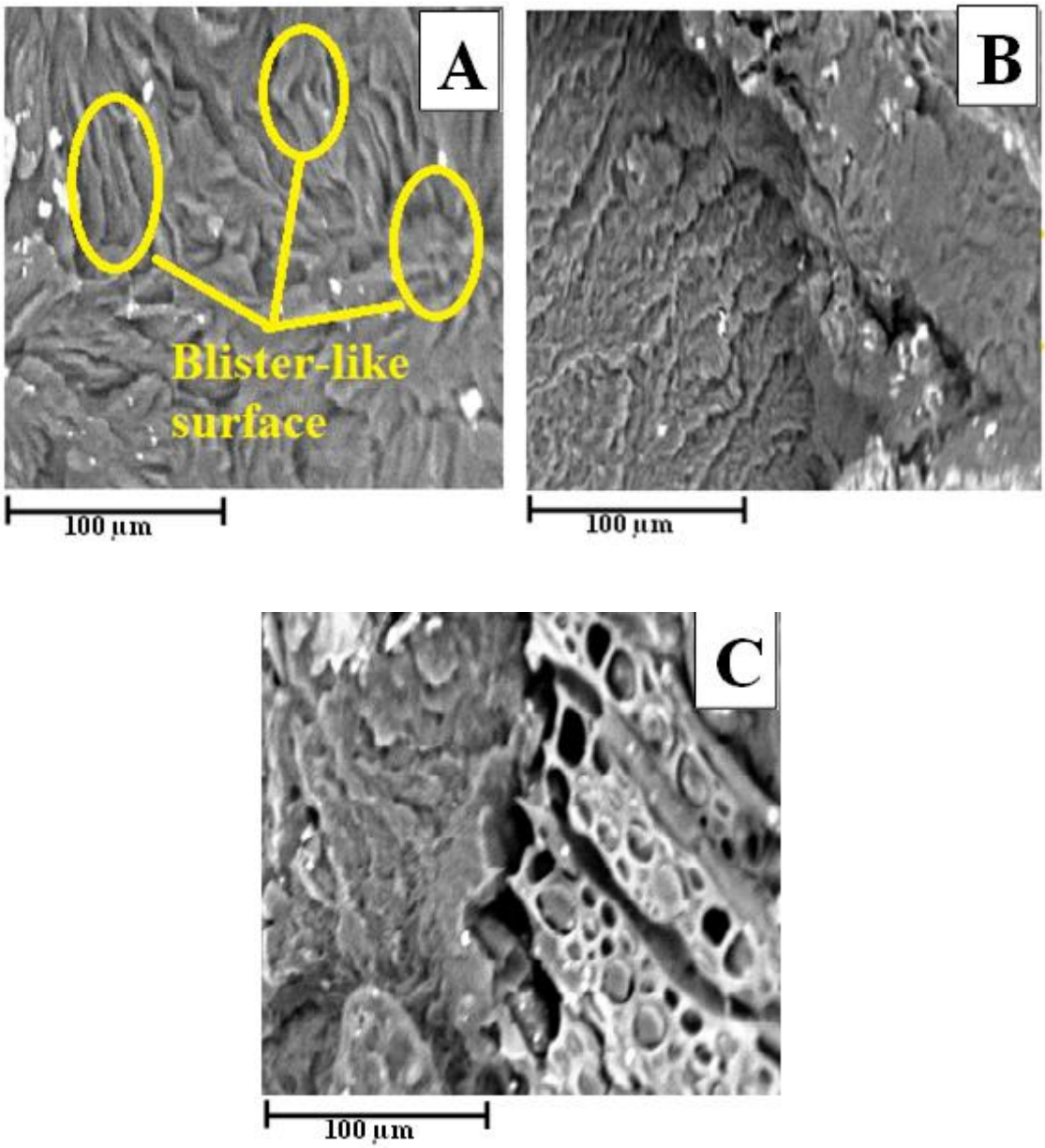

Fig.9. Fractured tensile test SEM images of (a) unreinforced LDPE (b) 70LDPE/30ALB$_p$ (150µm) (c) 70 LDPE/30 ALBp (408 µm) after 8th week of immersion in water.

4. CONCLUSION

This study has revealed other areas where ALB can be used asides its medicinal potentials. Additional peaks of 1644 (C=C) and 1057cm^{-1} (C-O-C) have imparted improved mechanical properties on LDPE with 150µm ALBp particles offering the best reinforcing effect. Poor matrix/reinforcement bonding is witnessed when 408µm ALBp are used as reinforcement. This leads to existence of cavities and voids thus imparting a less mechanical strengthening effect compared to LDPE reinforced with 150µm ALBp. Thermal stability and *X*c are improved with ALBp addition, 70LDPE/30ALBp (150µm) possessing the maximum values. In summary, the finer the ALBp, the better they serve as good reinforcements on LDPE.

5. REFERENCES

Abdul Rahman, N.H., Chieng, B.W., Ibrahim, N.A. and Abdul Rahman, N. (2012) "Extraction and characterization of cellulose nanocrystals from tea leaf waste fibers", Polymers, 9, 1-11.

Adeosun, S.O., Gbenebor, O.P., Akpan, E.I. and Udeme, F. (2015) "Influence of organic fillers on physicochemical and mechanical properties of unsaturated polyester composites", Arabian Journal of Science and Engineering, 41, 4153-4159.

Adeosun, S.O., Taiwo, O., Akpan, E.I., Gbenebor, O.P., Gbagba, S. and Olaleye, O. (2016) "Mechanical characteristics of groundnut shell particle reinforced polylactide nano fibre", RevistaMateria, 21(2), 482-491.

Bilyeu, B., Brostow, W. and Menard, K.P. (2001) "Determination of volume changes during cure via void elimination and shrinkage of an epoxy prepreg using a quartz dilatometry cell", Polimer, 46(7), 99-802.

Chun, K.S., Husseinsyah, S. and Syazwani, N.F. (2015) "Properties of kapok husk-filled linear low-density polyethylene ecocomposites: Effect of polyethylene-grafted acrylic acid", Thermoplastic Composite Materials, 1-15.

Flandez, J., Gonzalez, I., Resplandis, J.B., Mansouri, N., Vilaseca, F. and Mutje, P. (2012) "Management of corn stalk waste as reinforcement for polypropylene injection moulded composites". Bioresources, 7(2), 1837-1849.

Gupta, N., Singh Brar, B. and.Woldesenbet, E. (2001) "Effect of filler addition on the compressive and impact properties of glass fibre reinforced epoxy", Bulletin of Materials Science. 24(2), 219-223.

Huang, R., Xu, X., Lee, S., Zhang, Y., Kim, B. and Wu., Q. (2013) "High density polyethylene composites reinforced with hybrid inorganic fillers: morphology, mechanical and thermal expansion performance", Materials., 6, 4122-4138.

Ishidi.Y.E. (2014) "Mechanical properties and micro-structural studies of some agrowaste – HDPE composites", Journal of Chemistry and Materials Research, 1(1), 2-6.

Kim, J., Kang, P.H. and Nho, Y.C. (2004) "Positive temperature coefficient behaviour of polymer composites having a high melting temperature" Journal of Applied Polymer Science, 92(1), 394-401.

Nazneen, M.B., Wesley, E.G. and Johnson, M. (2012) "FT-IR studies on the leaves of *a*lbizia lebbeck benth", International Journal of Pharmacy and Pharmaceutical Sciences, 4(3), 293-296

Raju, C.U., Kumarappa, S. and Gaitonde, VN. (2012) ".Mechanical and physical characterization of agricultural waste reinforced polymer composites", Journal of Material and Environmental Sciences, 3(5), 907-916.

Shahid, S.A. and Firdou, N. (2012) "Antimicrobial screening of albizia lebbeck (l.) benth. And acacia leucophloea (roxb.). African Journal of Pharmacy and Pharmacology", 6(46) 3180-3183.

Sabu, T., Kuruvilla, J., Sant, M., Koichi, G. and Meyyarappallil, S. (2012) "Polymer composites", Wiley-VCH Verlag GmbH & Co. KGaA. 1 - 16.

Shehu, U., Aponbiede, O., Ause, T. and Obiodunukwe, E.F. (2014) "Effect of particle size on the properties of polyester/palm kernel shell (pks) particulate composites", Journal of Materials and Environmental Sciences. 5(2), 366-373.

Uygunoglu, T., Gunes, I. and Brostow, I.W. (2015) "Physical and mechanical properties of polymer composites with high content of wastes including boron", Materials Research, 18(6), 1188-1196.

Wan, Y.J., Gong, L.X., Tang, L.C., Wu, L.B. and Jiang, J.X. (2014) "Mechanical properties of epoxy composites filled with silane-functionalized graphene oxide", Composites Part A, Applied Science and Manufacturing, 64, 79-89.

Wang,, Y., Chang,, Y., Yu,, L., Zhang,, C., Xu, X.,. Xue, Y., Li. Z. and Xue, C. (2013) "Crystalline structure and thermal property characterization of chitin from Antarctic krill (Euphausia superba)", Carbohydrate Polymers, 92, 90– 97.